

Journal of Experimental Botany, Vol. 75, No. 15 pp. 4655–4670, 2024 https://doi.org/10.1093/jxb/erae235 Advance Access Publication 30 May 2024



RESEARCH PAPER

Arabidopsis transcription factor ANAC102 predominantly expresses a nuclear protein and acts as a negative regulator of methyl viologen-induced oxidative stress responses

Xiaopeng Luo^{1,2,1}, Xinqiang Jiang^{1,2,3,1}, Vivian Schmitt^{4,1}, Shubhada R. Kulkarni^{1,2,5,6}, Huy Cuong Tran^{4,1}, Sylwia M. Kacprzak^{4,1}, Frank Van Breusegem^{1,2,1}, Olivier Van Aken^{4,1}, Klaas Vandepoele^{1,2,7}, And Inge De Clercq^{1,2,*},

- ¹ Ghent University, Department of Plant Biotechnology and Bioinformatics, 9052 Ghent, Belgium
- ²VIB Center for Plant Systems Biology, 9052 Ghent, Belgium
- ³ College of Landscape Architecture and Forestry, Qingdao Agricultural University, Qingdao, 266109, Shandong, China
- ⁴ Department of Biology, Lund University, Lund 223 62, Sweden
- ⁵ European Center for Angioscience, Medical Faculty Mannheim, Heidelberg University, Heidelberg, Germany
- ⁶ Division of Vascular Oncology and Metastasis, German Cancer Research Center Heidelberg (DKFZ-ZMBH Alliance), Heidelberg, Germany
- ⁷ VIB Center for AI & Computational Biology, VIB, Ghent, Belgium
- * Correspondence: inge.declercq@psb.vib-ugent.be

Received 13 February 2024; Editorial decision 17 May 2024; Accepted 29 May 2024

Editor: Saijaliisa Kangasjärvi, University of Helsinki, Finland

Abstract

Plants, being sessile organisms, constantly need to respond to environmental stresses, often leading to the accumulation of reactive oxygen species (ROS). While ROS can be harmful, they also act as second messengers guiding plant growth and stress responses. Because chloroplasts are sensitive to environmental changes and are both a source and a target of ROS during stress conditions, they are important in conveying environmental changes to the nucleus, where acclimation responses are coordinated to maintain organellar and overall cellular homeostasis. ANAC102 has previously been established as a regulator of β-cyclocitral-mediated chloroplast-to-nucleus signaling, protecting plants against photooxidative stress. However, debates persist about where ANAC102 is located—in chloroplasts or in the nucleus. Our study, utilizing the genomic *ANAC102* sequence driven by its native promoter, establishes ANAC102 primarily as a nuclear protein, lacking a complete N-terminal chloroplast-targeting peptide. Moreover, our research reveals the sensitivity of plants overexpressing *ANAC102* to severe superoxide-induced chloroplast oxidative stress. Transcriptome analysis unraveled a dual role of ANAC102 in negatively and positively regulating genome-wide transcriptional responses to chloroplast oxidative stress. Through the integration of published data and our own study, we constructed a comprehensive transcriptional network, which suggests that ANAC102 exerts direct and indirect control over transcriptional responses through downstream transcription factor networks, providing deeper insights into the ANAC102-mediated regulatory landscape during oxidative stress.

Abbreviations: β -cc, β -cyclocitral; p35S, cauliflower mosaic virus 35S promoter; ChI, chlorophyll; cTP, chloroplast-targeting peptide; DEG, differentially expressed gene; GO, Gene Ontology; IP, immunoprecipitation; KO, knockout; OE, overexpressing; MV, methyl viologen; MDS, mitochondrial dysfunction stimulon; MS, Murashige and Skoog; OE, overexpression; RT-qPCR, quantitative real-time PCR; ROS, reactive oxygen species; RNA-seq, RNA-sequencing; TE, Tris-EDTA; TF, transcription factor; TIS, translation initiation site; TSS, transcription start site; WT, wild type; Y1H, yeast one-hybrid.

Keywords: Arabidopsis, chloroplasts, gene regulatory networks, oxidative stress, retrograde signaling, transcription factors.

Introduction

Due to their sedentary nature, plants must continuously acclimate to changing environmental conditions, such as temperature shifts, water availability, and high light levels, which often lead to the accumulation of reactive oxygen species (ROS) within the plant. Excessive ROS accumulation can disrupt redox homeostasis and causes progressive oxidative damage, ultimately leading to cell death. Conversely, ROS can serve as signaling molecules, acting as second messengers extensively coordinating plant growth, development, and acclimation in response to environmental as well as intracellular changes (Gechev et al., 2006; Baxter et al., 2014; Considine and Foyer, 2021; Mittler et al., 2022). During stresses, ROS production is increased in organelles due to perturbation of their metabolic processes such as photosynthesis, photorespiration, and/or respiration. To counteract oxidative stress and to maintain cellular energy homeostasis, activities of the organelles are tightly coordinated with the transcriptional machinery in the nucleus. This involves both anterograde regulation (signaling from the nucleus to organelles) and retrograde signaling (communication from organelles to the nucleus) (Woodson and Chory, 2008).

Due to the sensitivity of chloroplastic processes to various stresses, chloroplasts are thought to serve as crucial sensors and intermediaries between environmental fluctuations and responses in the nucleus (Crawford et al., 2018; Schwenkert et al., 2022). Stress-triggered chloroplast retrograde signals are mediated by ROS, metabolites including β-cyclocitral 2-C-methyl-D-erythritol 2,4-cyclodiphosphate, 3'-phosphoadenosine 5'-phosphate, and intermediates of the tetrapyrrole biosynthesis pathway (Moulin et al., 2008; Estavillo et al., 2011; Ramel et al., 2012; Xiao et al., 2012; Terry and Smith, 2013; Dietz et al., 2016; Exposito-Rodriguez et al., 2017). ANAC102 has been identified as a key player in β -cc-mediated chloroplast retrograde signaling, positioned upstream of at least three other NO APICAL MERISTEM/ARABIDOPSIS ACTIVATION TRANSCRIPTION FACTOR/CUP-SHAPED COTYLEDON (NAC) transcription factors (TFs) (ANAC002, ANAC032, and ANAC081), inducing a detoxification response and facilitating plant acclimation to photooxidative stress (D'Alessandro et al., 2018). Simultaneously, ANAC102 has been implicated in cadmium (Cd) tolerance, in plant growth during mild methyl viologen (MV)-induced oxidative stress, and in protecting germinating seeds against low oxygen stress (Christianson et al., 2009; De Clercq et al., 2021; Han et al., 2023). Despite its essential functions, there is an ongoing debate regarding the subcellular localization of ANAC102. Initial reports, based on the expression of the annotated coding sequence (ANAC102.1) from the cauliflower mosaic virus 35S promoter (p35S), in both Arabidopsis

thaliana and Nicotiana benthamiana, suggested that ANAC102 is a chloroplast-localized TF (Inzé et al., 2012). Subsequent research contended that ANAC102 is present in both the nucleus and chloroplasts, in the latter compartment interacting with RNA polymerases to regulate the transcription of chloroplast genes (Xin et al., 2021). Recent findings reported a nuclear localization and function for ANAC102 by binding to the promoter and regulating expression of a gene involved in Cd stress responses (Han et al., 2023). Moreover, ANAC102 was observed to exclusively localize in the nucleus when expressed without the predicted N-terminal chloroplast-targeting peptide (cTP), which was found to be sufficient for chloroplast targeting (Inzé, 2012; Xin et al., 2021). Adding to the complexity, ANAC102 has been reported to possess two transcription start sites (TSSs) that are alternatively selected during red light exposure (Ushijima et al., 2017). While the two mRNA models according to TAIR10 (ANAC102.1 and ANAC102.2; arabidopsis.org; Fig. 1A) include the cTP in the coding sequence, both TSSs identified by Ushijima et al. (2017), respectively positioned within and downstream of the cTP, exclude expression of the complete cTP.

A complete view on the different TSSs and whether the corresponding protein model(s) include the (complete) cTP, remain unclear. Therefore, we investigated the subcellular localization of ANAC102 using its genomic sequence controlled by its native promoter. Our findings revealed that ANAC102 predominantly expresses a nuclear protein isoform, omitting the N-terminal extension containing the cTP. Furthermore, our observations indicate that ANAC102 serves as a negative and positive regulator of MV-induced chloroplast retrograde signaling in the nucleus, both directly through transcriptional regulation of target genes and indirectly through TF networks.

Materials and methods

Plant material and growth conditions

Arabidopsis thaliana seedlings were grown at 21 °C under a 16 h light/8 h dark photoperiod on half-strength Murashige and Skoog (1/2 MS) medium (Duchefa Biochemie, Haarlem, The Netherlands), supplemented with 1% (w/v) sucrose, 0.75% (w/v) agar, and adjusted to pH 5.7, following stratification for 48 h. The Arabidopsis lines overexpressing (OE) the full-length ANAC102.1 (AT5G63790, TAIR, arabidopsis.org)-coding sequence from the p35S in the Col-0 background have been described previously (Inzé, 2012). The T-DNA insertion lines for ANAC102 [SALK_030702C; anac102 knockout (KO)] were obtained from the European Arabidopsis Stock Centre. The homozygous T-DNA insertion line was confirmed by PCR with gene-specific primers (LP and RP) and a T-DNA-specific primer (LB; Supplementary Table S1). Quantitative real-time PCR (RT-qPCR) analysis indicated 1% residual ANAC102 mRNA levels compared to the wild type (WT). The translational fusion

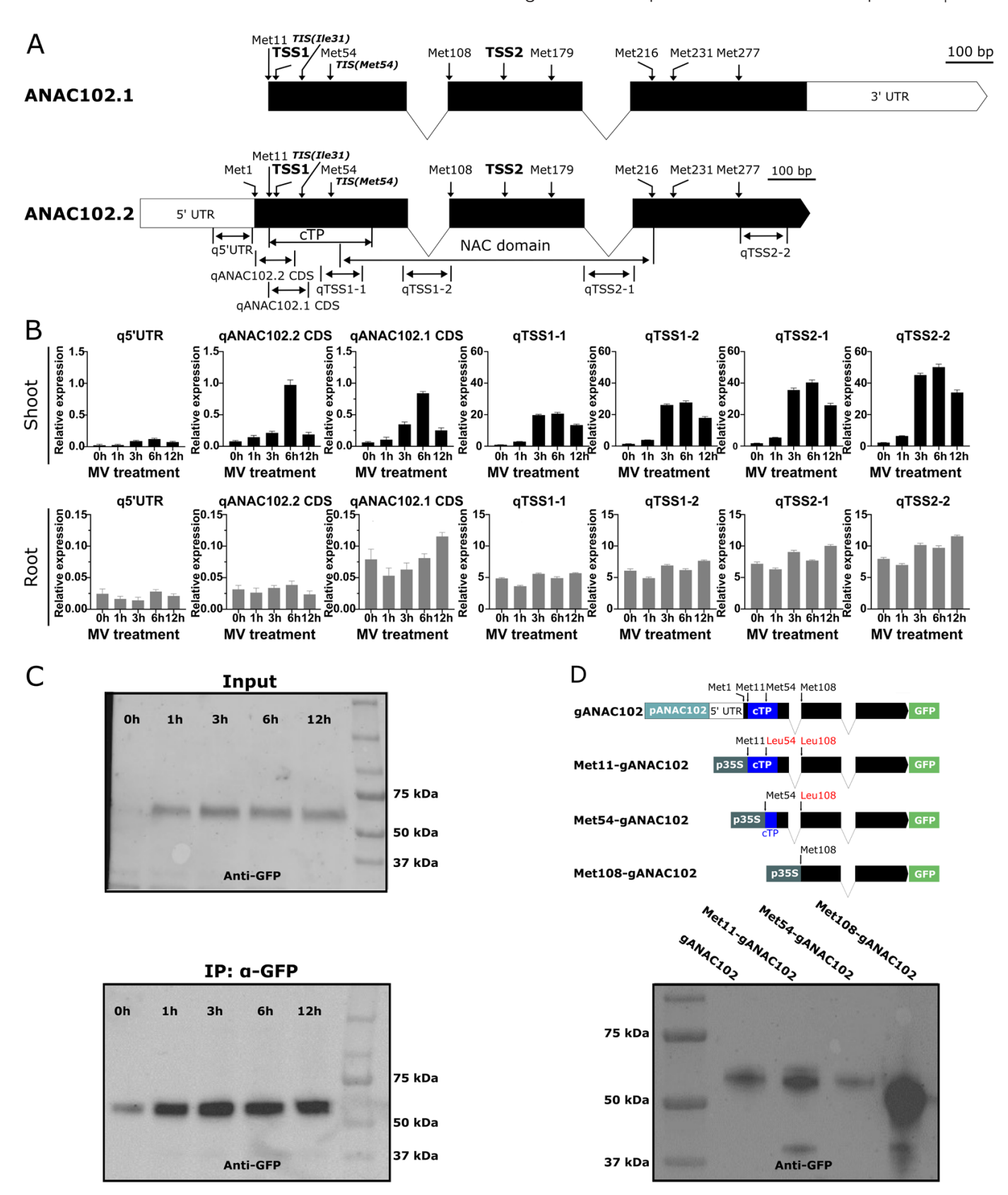


Fig. 1. ANAC102 predominantly expresses a nuclear protein isoform. (A) Overview of the ANAC102 gene model with transcription start sites (TSS1 and TSS2, identified by TSS-Seq, Ushijima et al., 2017 and Nielsen et al., 2019), potential in-frame AUG start codons (Met), and translation initiation sites (TIS, identified by Ribo-Seq profiling, Willems et al., 2022) indicated in the ANAC102.1 and ANAC102.2 transcript models (according to TAIR; arabidopsis.org).

4658 | Luo et al.

q, RT-qPCR amplicons to study the different *ANAC102* transcript models, corresponding to the 5'UTR, *ANAC102.2* coding sequence (CDS) and the *ANAC102.1* CDS regions, and the TSS1 and TSS2 transcript models, respectively; cTP, chloroplast-targeting peptide (80-amino-acid sequence, Xin *et al.*, 2021). (B) RT-qPCR analysis of the different *ANAC102* transcript models in *Arabidopsis thaliana* wild-type seedlings during an MV stress time series. Error bars represent the SD (*n*=4 biological replicates). (C) Western blot analysis of the ANAC102 protein model in total protein extracts, before (input) and after anti-GFP immunoprecipitation (IP), from Arabidopsis seedlings stably expressing the genomic *ANAC102* gene fragment [-1500 +1395] fused to GFP (pANAC102::gANAC102-GFP) during an MV stress time series. (D) Western blot analysis of the ANAC102 protein model after transient expression of pANAC102::gANAC102-GFP in *N. benthamiana* and comparison with different N-terminally truncated protein isoforms initiated at different in-frame AUG start codons (Met11, Met54, and Met108) and mutated in the downstream start codon(s) (Met54 and Met108).

constructs were obtained using Gateway cloning (Karimi et al., 2002). The 2895 bp genomic region comprising the 5' upstream regulatory region and genomic DNA of ANAC102 [–1500 + 1395] was amplified from Arabidopsis Col-0 genomic DNA using iProof high-fidelity DNA polymerase (Bio-Rad) and cloned into the pB7FWG destination vector (primers used are shown in Supplementary Table S1). The synthetic N-terminal truncated ANAC102 gene fragments, in which downstream Met residues (Met54, Met108) were mutated, were obtained with the BioXP3200 DNA printer and subsequently cloned into the pB7FWG2 destination vector. The constructs were transformed in A. thaliana WT Col-0 plants via Agrobacterium-mediated floral dipping (Clough and Bent, 1998).

Methyl viologen stress treatments

For the phenotypic analysis during MV stress, 2-week-old WT, ANAC102.1 OE (OE1 and OE2), and anac102 KO lines, grown together on a nylon mesh on 1/2 MS, were transferred to 1/2 MS medium supplemented with 2 μ M MV (Sigma-Aldrich). The maximum photosystem II efficiency ($F_{\rm v}'/F_{\rm m}'$) was determined with a PAM-2000 chlorophyll fluorometer and the ImagingWinGigE software application (Walz; Effeltrich, Germany) on light-adapted plants. For RT-qPCR and RNA-sequencing (RNA-seq) analyses on ANAC102.1 OE and KO lines, the same setup was used, except for using a higher MV concentration (50 μ M). For the RT-qPCR analysis of the Met54-gANAC102-GFP OE line and the ANAC102-green fluorescent protein (GFP), 2-week-old seedlings grown on 1/2 MS medium were sprayed with 50 μ M MV in water containing 0.1% Tween-20.

RNA isolation and RT-qPCR analysis

Total RNA extraction from 100 mg of plant material was conducted using the ReliaPrepTM RNA Tissue Miniprep System (Promega) including DNase treatment. cDNA was synthesized from 1 µg of total RNA using the qScript cDNA SuperMix kit (Quanta BioSciences, Belgium), which includes a precise combination of oligo(dT) and random primers. RT-qPCR analysis was performed using the SYBR Green I Master kit (Roche, Belgium) on a Roche LightCycler 480. The results were analyzed with the 2-ADCt method (Livak and Schmittgen, 2001). For the analysis of the ANAC102 transcript models, two reference genes, UBIQUITIN-CONJUGATING ENZYME 21 (UBC21) and ACTIN7 (ACT7), were used for normalization. For the normalization of the MDS (mitochondrial dysfunction stimulon) gene expression levels, ACTIN-RELATED PROTEIN7 (ARP7) (ANAC102.1 OE lines) or both UBC21 and ACTIN7 (Met54-gANAC102-GFP OE lines) were used. Stability of the expression of the reference genes was assessed under all experimental conditions (Supplementary Fig. S1). Results are based on four biological replicates for the transcript model analysis, and two and three biological replicates for the MDS gene expression analyses in ANAC102.1 OE and Met54-gANAC102-GFP OE lines, respectively. The RT-qPCR primers (Supplementary Table S1) were designed by the online Primer-BLAST tool (https://www.ncbi.nlm.nih.gov/tools/primer-blast/).

Confocal imaging

For the subcellular localization analysis, the translational fluorescent reporter constructs were transformed into *Agrobacterium tumefaciens* GV3101 through electroporation. Subsequently, these *Agrobacterium* strains were infiltrated together with the RNA silencing inhibitor p19 in 4-week-old *N. benthamiana* epidermal cells and analyzed 3 d after infiltration (Li, 2011). Subcellular localization analysis in Arabidopsis lines stably transformed with the translational fluorescent reporter lines was performed on root tissue of 5-day-old seedlings. Imaging was performed on a Leica SP8 confocal microscope equipped with an HC PL APO CS2 × 40 water-corrected immersion objective. GFP was excited at 488 nm and captured between 515 nm and 545 nm. Chlorophyll (Chl) autofluorescence was excited at 561 nm and detected at 560–630 nm.

Protein extraction, immunoprecipitation, and western blot analysis

A 1 g aliquot of plant tissue (whole seedlings of Arabidopsis and leaf tissue of N. benthamiana) was ground in liquid nitrogen and dissolved in protein extraction buffer [150 mM Tris-HCl pH 7.5, 150 mM NaCl, 1% (v/v) NP-40, 10% (v/v) glycerol, 10 mM EDTA, 1 mM sodium molybdate, 1 mM phenylmethylsulfonyl fluoride (PMSF), cOmpleteTM protease inhibitor cocktail (Roche)]. The homogenate was centrifuged for 30 min at 4 °C to eliminate cell debris. The protein extract supernatant was collected and incubated with 40 µl of GFP-Trap Magnetic Agarose beads (Chromotek) for 2 h at 4 °C. The solution was removed and the beads were washed three times for 1 min with 700 µl of washing buffer (20 mM Tris-HCl pH 7.5, 150 mM NaCl). Elution was performed by mixing the beads with 40 µl of ultra-pure MO H₂O and 10 µl of 5× Laemmli sample buffer [10% SDS, 25% 2-mercaptoehtanol, 50% glycerol, 0.01% (w/v) bromophenol blue, 312.5 mM Tris-HCl (pH 6.8)] and heating for 10 min at 95 °C. Immunopurified protein eluates and total protein extracts were loaded and separated on a 4-20% SDS-PAGE gel, transferred to a polyvinylidene fluoride (PVDF) membrane, blocked, and blotted with anti-GFP-horseradish peroxidase (HRP) (5000-fold dilution) (Miltenyi Biotec) using the Western Lightning kit (GE-Healthcare). Blots were imaged using the BioRad Chemidoc system.

Yeast one-hybrid screening

Yeast strain YM4271 and destination vector pMW#2 were obtained from Dr M. Walhout (University of Massachusetts Medical School, Worcester, MA, USA). The REGIA collection was provided by Dr Franziska Turck (Max Planck Institute for Plant Breeding Research, Köln, Germany). Design of the yeast reporter strains was done as described in detail (Deplancke *et al.*, 2006). Primers used for cloning of the promoters are displayed in Supplementary Table S1. For the screening of the REGIA collection, the 1394 prey plasmids were individually transformed in the reporter yeast strains by means of a high-throughput transformation system in the 96-well format (Deplancke *et al.*, 2006; Vermeirssen *et al.*, 2007). A 20 µl aliquot of competent yeast cell suspension, 100 ng of

plasmid, and 100 µl of Tris-EDTA (TE)/lithium acetate/polyethyleneglycol were combined per well. After heat shock (20 min at 30 °C), plates were centrifuged (for 10 s) and the supernatant was removed. Yeast cells were resuspended in 20 µl of TE, of which 5 µl was spotted on selective (SD-His-Ura-Trp; Clontech) medium and on SD-His-Ura-Trp containing the appropriate concentration of 3-aminotriazole (3-AT) (Acros Organics) to minimize autoactivation. Growth on 3-AT was monitored during 3-10 d after transfer. Interactions were confirmed by retransforming the isolated prey plasmids in the yeast reporter strains and analyzing a 10- and 100-fold dilution on SD-His-Ura-Trp medium supplemented with 3-AT.

RNA-sequencing sample preparation and data analysis

ANAC102.1 OE, anac102 KO, and WT lines were sown together on a mesh placed on 1/2 MS medium and grown at a light intensity of 55-60 μmol m⁻² s⁻¹, with a light cycle of 16 h light/8 h dark. Subsequently, 2-week-old seedlings on the nylon mesh were transferred to 1/2 MS medium containing 50 µM MV or to normal 1/2 MS medium (mock). Shoot tissue of 5-6 seedlings was harvested for RNA extraction at 12 h after transfer. RNA concentration and purity were determined spectrophotometrically using a Nanodrop ND-1000 (Nanodrop Technologies) and RNA integrity was assessed using a Bioanalyzer 2100 (Agilent). Per sample, an amount of 1 µg of total RNA was used as input. Using the Illumina TruSeq® Stranded mRNA Sample Prep Kit (protocol version: Part # 1000000040498 v00 October 2017), poly(A)-containing mRNA molecules were purified from the total RNA input using poly(T) oligoattached magnetic beads. In a reverse transcription reaction using random primers, RNA was converted into first-strand cDNA and subsequently converted into double-stranded cDNA in a second strand cDNA synthesis reaction using DNA polymerase I and RNase H. The cDNA fragments were extended with a single 'A' base to the 3' ends of the bluntended cDNA fragments, after which multiple indexing adapters were ligated introducing different barcodes for each sample. Finally, a PCR was carried out to enrich those DNA fragments that have adapter molecules on both ends and to amplify the amount of DNA in the library. Sequence libraries of each sample were equimolarly pooled and sequenced on an Illumina NextSeq 500 (High Output Flowcell, 75 bp, Single Reads, v2.5) at the VIB Nucleomics Core (www.nucleomicscore.sites.vib.be). Data were processed using demultiplexing and quality controlled with FastQC. Alignment of reads was performed against the TAIR10 annotation using STAR (Dobin et al., 2013). On average, 20 million reads per sample were mapped to the Arabidopsis genome. Counts were assigned to genes using featureCounts (Liao et al., 2014), and analysis of differentially expressed genes (DEGs) was performed with DeSEQ2, modeling for batch effects, without independent filtering and Cooks filter (Love et al., 2014). Transcripts were considered differentially expressed if the adjusted P-value was < 0.05.

Chromatin immunoprecipitation-sequencing data analysis

The ChIP-seq peaks for ANAC102 used in this study were adapted from Song et al. (2016). The peaks were annotated to the closest genes using the TAIR 10 gene annotation, only considering protein-coding genes and discarding peaks that were >2000 bp away from the closest gene or that were overlapping with coding exons.

Chlorophyll measurements

Total Chl was extracted from shoots of 2-week-old ANAC102.1 OE, anac102 KO, and WT lines using 80% acetone, and measured using a spectrophotometer at wavelengths of 645 nm and 663 nm according to Arnon (1949). The Chl index was measured based on reflectance at 710 nm and 770 nm (Gitelson et al., 2003) using a multispectral

phenotyping platform. RGB (red green blue) images were processed via the 'Data Analysis Software' program (Phenovation BV, Wageningen, The Netherlands).

Results

ANAC102 mainly expresses a nuclear protein isoform without a full-length N-terminal chloroplast-targeting peptide

To evaluate and quantify different potential ANAC102 transcript models, we analyzed different regions in the ANAC102 genomic sequence via RT-qPCR. Four RT-qPCR primer pairs (qTSS1-1, qTSS1-2, qTSS2-1, and qTSS2-2; Supplementary Table S1) were designed downstream of the two TSSs (TSS1 and TSS2; Fig. 1A) previously identified by TSS-Seq (Ushijima et al., 2017; Nielsen et al., 2019), in addition to two upstream primer pairs encompassing the 5' end of the ANAC102.2 and ANAC102.1 coding sequences (CDSs) in the TSS1 upstream region (qANAC102.2 CDS and qANAC102.1 CDS; Supplementary Table S1) and one targeting the 5'-untranslated region (q5'UTR; Fig. 1A; Supplementary Table S1). We analyzed shoot and root tissue of Arabidopsis WT seedlings grown under control conditions or treated with MV for 1, 3, 6, and 12 h. MV, which generates ROS mainly in the chloroplasts under light conditions, is generally considered to trigger chloroplast retrograde signaling and increases ANAC102 transcript levels (Zimmermann et al., 2004; Ugalde et al., 2021). Under non-treated conditions (0 h), the region downstream of TSS1 (qTSS1-1) showed ~15-fold (shoot tissue) and 61-fold (root tissue) higher expression compared to the region directly upstream of TSS1 (qANAC102.1 CDS) (Fig. 1B). This indicates that TSS1 is a predominant TSS, which is consistent with a recent study (Cresta and D'Alessandro, 2023). In addition, the 5'-extended transcripts (q5'UTR, qANAC102.2 CDS, and qANAC102.1 CDS) showed an overall milder MV induction pattern in leaf tissue compared to the earlier and stronger onset of the MV response of the shorter TSS1 and TSS2 transcripts (Fig. 1B). This is in agreement with the study by Cresta and D'Alessandro (2023), who investigated the responsiveness of different ANAC102 isoforms to β-cc and photorespiratory stress, reporting no or a reduced induction of the larger, 5'-elongated ANAC102 isoform.

The transcript abundance of the region immediately downstream of TSS1 (qTSS1-1) was comparable to that of the more downstream qTSS1-2 under both control and stress conditions, implying the absence of additional TSSs between TSS1 and the second, downstream TSS2. Analysis of the transcript abundance using primers targeting the TSS2 downstream region (qTSS2-1 and qTSS2-2) revealed higher (~1.7-fold in shoot and ~1.4-fold in root) expression levels compared to qTSS1-1 and qTSS1-2 (Fig. 1B), indicating that TSS2 might represent an additional TSS downstream of TSS1. However, the dynamics of stress induction were similar between the TSS1

and TSS2 transcripts. In summary, the TSS1 and TSS2 transcripts, both leading to protein isoforms that (probably) lack a functional cTP, are predominantly expressed, constituting 95% and 99% of the total transcript under control conditions in shoot and root tissues, respectively. Moreover, although the TSS1 and TSS2 transcripts were the main isoforms under both control and stress conditions, a minor portion of the total transcript still encoded a larger, 5'-extended transcript, indicating that a chloroplastic ANAC102 proteoform might still exist.

To further unravel the 5'-extended transcript model(s), we analyzed the TSS1 upstream regions (q5'UTR, qANAC102.2 CDS, and qANAC102.1 CDS). In shoot tissue, qANAC102.2 CDS and qANAC102.1 CDS showed similar expression levels, under both control and stress conditions, whereas the transcript levels corresponding to the 5'UTR were considerably lower. In root tissue, qANAC102.1 CDS had ~2- to 3-fold higher transcript levels compared to both q5'UTR and qANAC102.2 CDS, which had similar expression levels. These results suggest that there may be different TSSs in the ANAC102 5' region and that these TSSs are differentially utilized between root and shoot tissue. However, the specifics of the protein models corresponding to the different transcript isoforms, including the translation initiation site (TIS) usage, remain unclear.

To evaluate the ANAC102 protein model, we used the full genomic ANAC102 gene fragment [-1500 + 1395] containing the 1,262-kb upstream regulatory region, the 5'UTR, and all exons and introns, translationally fused (pANAC102::gANAC102-GFP). We analyzed the resulting protein isoform(s) in stably transformed pANAC102::gANAC102-GFP Arabidopsis lines, before and after a 1, 3, 6, and 12 h MV treatment. Protein immunoblot analysis of total protein extracts before and after enrichment by anti-GFP immunoprecipitation (IP) revealed only a single protein isoform under both control and stress conditions (Fig. 1C). Comparison with different N-terminally truncated ANAC102 protein isoforms initiated at different in-frame start codons (Met11, Met54, and Met108, Fig. 1A) after transient expression in N. benthamiana indicated that translation probably occured from Met54, the first in-frame AUG start codon downstream of TSS1. This protein isoform lacks the full cTP (Fig. 1A) and accordingly resulted in an exclusively nuclear localization pattern in roots of stably transformed pANAC102::gANAC102-GFP Arabidopsis plants and in leaves of N. benthamiana after transient expression of this construct (Supplementary Fig. S2). Although we did not detect any additional bands before and after enrichment by IP, either under control or MV stress conditions in which the abundance of ANAC102 mRNA and protein was increased, we cannot exclude that a longer, N-terminal-extended protein isoform is generated, albeit at levels we cannot detect with western blot performed on total protein extracts. Overexpression of the genomic fragment starting at Met11 (Met11-gANAC102-GFP) resulted in three protein bands (Fig. 1D) and in a dual chloroplast-nuclear localization in N. benthamiana leaves and a nuclear localization in Arabidopsis roots (Supplementary Fig. S2B). The largest protein isoform might correspond to the expected full-length Met11gANAC102-GFP protein (~63 kDa) whereas the slightly smaller proteoform might correspond to the chloroplastimported protein with the cTP cleaved off. Although the two in-frame, downstream AUGs (Met54 and Met108) were mutated in the Met11-gANAC102-GFP construct, we cannot exclude that the observed short isoform is generated by alternative (non-AUG) translation initiation downstream of Met11, directly generating a cTP-depleted, nuclear isoform. Interestingly, the smallest ~40 kDa proteoform, which was also detected in Met108-gANAC102-GFP, might be the result of translation from the TSS2 transcript. However, it was not obtained from the genomic pANAC102::gANAC102-GFP construct. Therefore, the protein isoform(s) resulting from the TSS2 transcript and the question of whether they originate from the same ORF remain unresolved.

Our results suggest that Met54 is the predominant TIS resulting in a protein isoform that contains the full NAC domain, but lacks the complete cTP. However, we cannot rule out the possibility that our method is not sensitive enough to detect the N-terminally extended proteoform(s) resulting from translation from the 5'-extended mRNA, which represents only a minor fraction of the total ANAC102 transcript pool. Similarly, a previous ribosome profiling study identified AUG(Met54) as the predominant TIS in addition to an inframe non-canonical (non-AUG) upstream TIS, AUU(Ile31) (Fig. 1A; Supplementary Fig. S3) (Willems et al., 2022). This non-canonical TIS is also located downstream of TSS1, but it remains to be investigated whether this results in a proteoform with a functional cTP or alternatively produces a nuclear isoform. We hypothesize that the dominant protein isoform is the nuclear ANAC102 version translated from Met54 and therefore we will further focus on its function in the nucleus.

ANAC102 overexpression increases sensitivity to severe methyl viologen stress

Our previous results have shown that ANAC102 affects seedling growth under mild MV-induced oxidative stress conditions (De Clercq et al., 2021). To assess the performance of ANAC102 gain- and loss-of-function lines under prolonged and more severe chloroplastic oxidative stress, we subjected ANAC102.1 OE1 and OE2 [~8-fold and ~80-fold overexpression of the ANAC102.1 (arabidopsis.org) CDS containing the cTP (Inzé, 2012) (Fig. 2A)] and anac102 KO (SALK_030702) plants to MV stress by placing 2-week-old seedlings on medium supplemented with 2 µM MV. Rosette growth and PSII efficiency (F_v'/F_m') were monitored at 7-d intervals. No significant differences were observed between the WT and the anac102 KO line (Fig. 2B, C). However, both ANAC102.1 OE1 and OE2 showed signs of stress from 21 days after treatment, which eventually lead to plant death at 5 weeks post

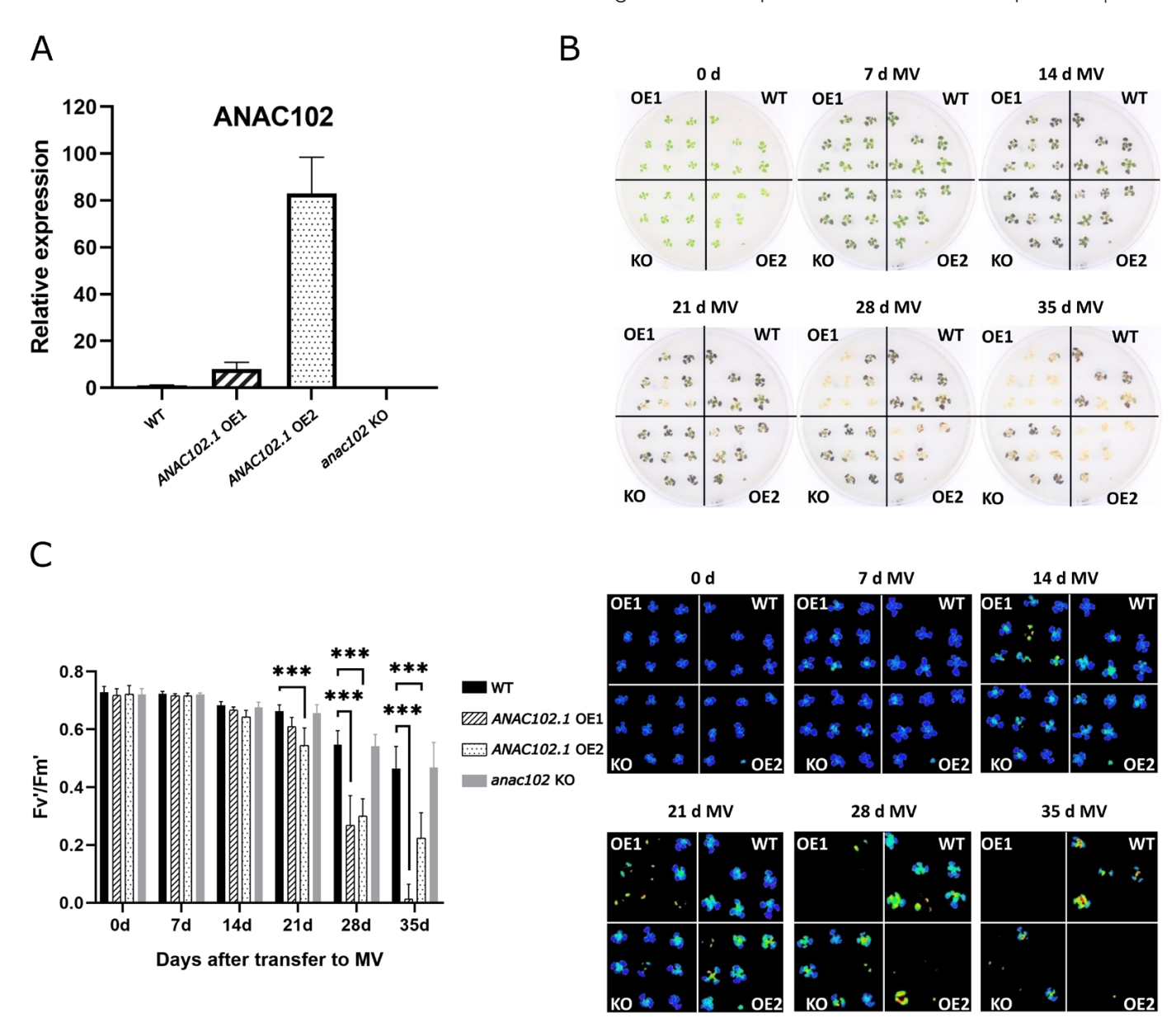


Fig. 2. Phenotype of ANAC102.1 OE and anac102 KO plants under severe methyl viologen (MV)-induced oxidative stress. (A) Expression levels of ANAC102 in ANAC102.1 overexpression (OE1 and OE2) and anac102 knockout (KO) lines relative to the wild type (WT). (B) Two-week-old WT, independent transgenic ANAC102 OE1 and OE2, and anac102 KO lines grown under control conditions were transferred to medium containing 2 µM MV. Rosette growth was visually monitored from transfer to MV (0 d) until 35 d after transfer. (C) Quantification of the light-adapted efficiency of PSII (F_v'/F_m') at different days after MV treatment and corresponding false color images. Error bars indicate the SD (n=15 biological replicates). Asterisks indicate significant differences to the WT (***P<0.001; two-way ANOVA with Tukey's multiple comparisons test).

treatment, in contrast to prolonged survival of the WT and anac102 KO plants (Fig. 2B). Additionally, F_v'/F_m' values of the ANAC102.1 OE lines, especially the younger leaves, showed a significant decline from 21 d after treatment compared to both the WT and anac102 KO plants (Fig. 2C).

Since the ANAC102.1 OE lines overexpress both the chloroplastic and nuclear ANAC102 proteins (Supplementary Fig. S2), we evaluated whether the MV susceptibility phenotype was due to increased activity of ANAC102 in the nucleus. We repeated the MV stress assays with a p 35S::Met54-gANAC102-GFP line

overexpressing only the cTP-depleted, nuclear isoform (10fold, Supplementary Fig. S4). Similar to the ANAC102.1 OE lines, the Met54-gANAC102-GFP OE line displayed earlier and more severe stress symptoms compared to WT plants, as evidenced by accelerated bleaching of the plants and decreased F_v'/F_m' from 2 weeks after transfer to MV (Supplementary Fig. S4). In conclusion, overexpression of ANAC102 increases the sensitivity to severe MV-induced oxidative stress and this phenotype is mainly caused by the activity of ANAC102 in the nucleus.

ANAC102 is a repressor of methyl viologen-induced retrograde gene expression

Subsequently, we investigated whether MV-responsive genes in the nucleus are modulated in ANAC102 gain-of-function lines. Two-week-old WT and ANAC102.1 OE1 and OE2 lines were transferred to medium supplemented with 50 µM MV, and shoots were harvested before (0 h) and at different time points (6, 9, and 12 h) after MV treatment for RT-qPCR analysis. We examined the expression of MDS genes previously defined as common targets of mitochondrial and MV-induced chloroplast retrograde signaling and regulated by ANAC013 that positively impacts plant MV stress tolerance (De Clercq et al., 2013; Van Aken et al., 2016). As expected, MDS genes (AOX1a, DTX1, SOT12, UGT74E2, and UGT73C6) were induced by MV in both WT and ANAC102.1 OE1 and OE2 lines, and induction was prominent from 9 h after treatment (Fig. 3A). However, a comparative analysis between WT and ANAC102.1 OE lines indicated a partial repression of MV-induced expression of the MDS genes in the strong OE2 line and to a lesser extent in the weaker OE1 line. This indicates that ANAC102.1 OE partially represses MV responses in the nucleus and that the repression effect occurred in a dosedependent manner.

To further determine whether the impaired retrograde responsive gene expression is due to ANAC102 activity in the nucleus, we analyzed MDS gene expression in p35S::Met54gANAC102-GFP lines. Similar to the ANAC102.1 OE lines, MDS gene induction by MV was partially repressed in Met54-gANAC102-GFP OE compared to the WT (Supplementary Fig. S5).

We identified ANAC102 in a yeast one-hybrid (Y1H) screen for TFs that bind to retrograde target gene promoters, including the AOX1a, UGT74E2, and UPOX promoters, using the REGIA library of Arabidopsis TFs (Paz-Ares and REGIA Consortium, 2002). We specifically reassessed and confirmed these interactions in targeted Y1H assays, demonstrating that ANAC102 can indeed directly bind to the promoters of AOX1a, UGT74E2, and UPOX (Fig. 3B). Moreover, analysis of available ChIP-seq data (Song et al., 2016) (see the Materials and methods) indicated binding of ANAC102 to the AOX1a and UGT74E2 promoters in plants grown with or without abscisic acid treatment, but not to the DTX1, SOT12, UGT73C6, and UPOX promoters.

In conclusion, our study demonstrates that ANAC102 acts as a repressor of MV-induced retrograde gene expression, potentially through direct binding to the target promoters in the nucleus.

ANAC102 negatively and positively regulates genomewide transcriptional responses to methyl viologen stress

To assess whether and how ANAC102 affects genome-wide transcriptional responses to MV, an RNA-seq analysis was performed on ANAC102.1 OE2, anac102 KO, and WT plants treated with MV or mock treated. Since MV-induced MDS gene expression was significantly induced at 12 h after transfer

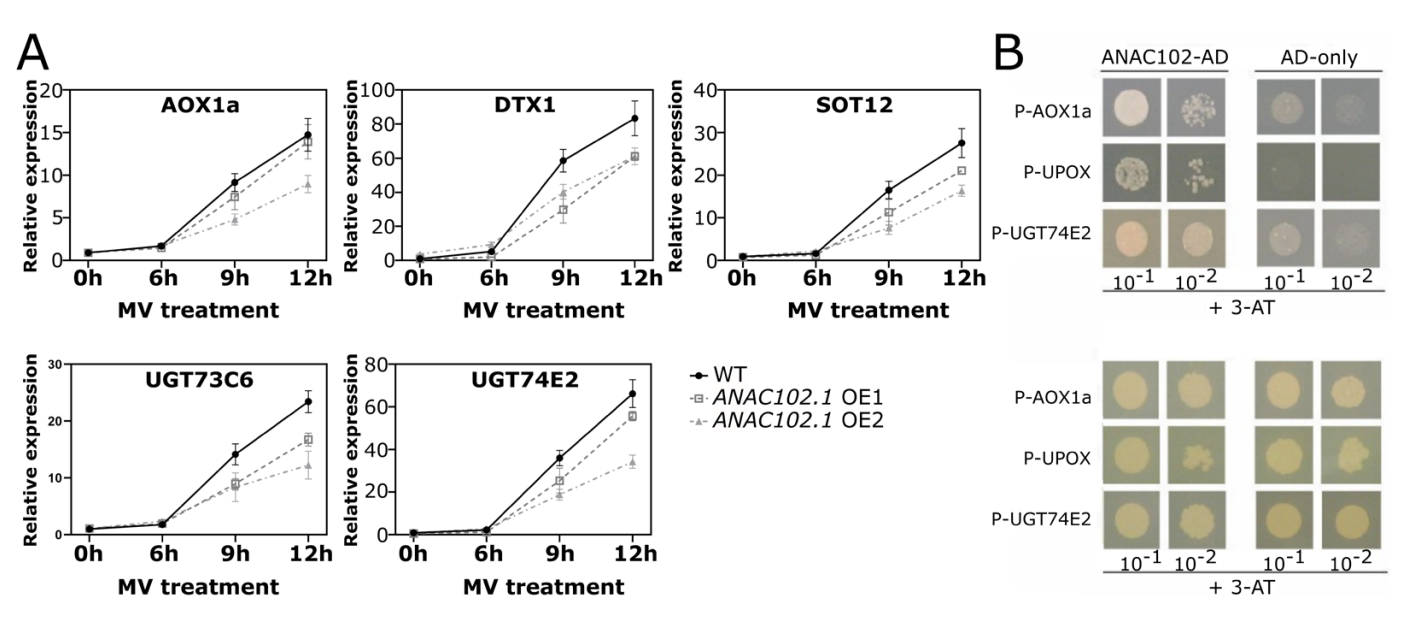


Fig. 3. ANAC102 negatively regulates MV-induced nuclear gene expression. (A) RT-qPCR analysis of retrograde target gene expression in the wild type (WT) and two independent ANAC102.1 OE lines (OE1, ~8-fold; and OE2, ~80-fold) during a metyl violgen (MV) treatment time course. Error bars indicate the SD (n=2 biological replicates). Similar data were obtained in at least two other biological repeat experiments. (B) Yeast one-hybrid analysis illustrating the binding of ANAC102 to retrograde target gene promoters. Yeast reporter strains, each containing the HIS3 reporter under the control of the AOX1a, UPOX, and UGT74E2 promoters and transformed with ANAC102 fused to either the GAL4 activation domain (ANAC102-AD) or the AD only (AD), were grown in the presence or absence of minimal 3-AT concentrations (5-20 mM) to suppress autoactivation.

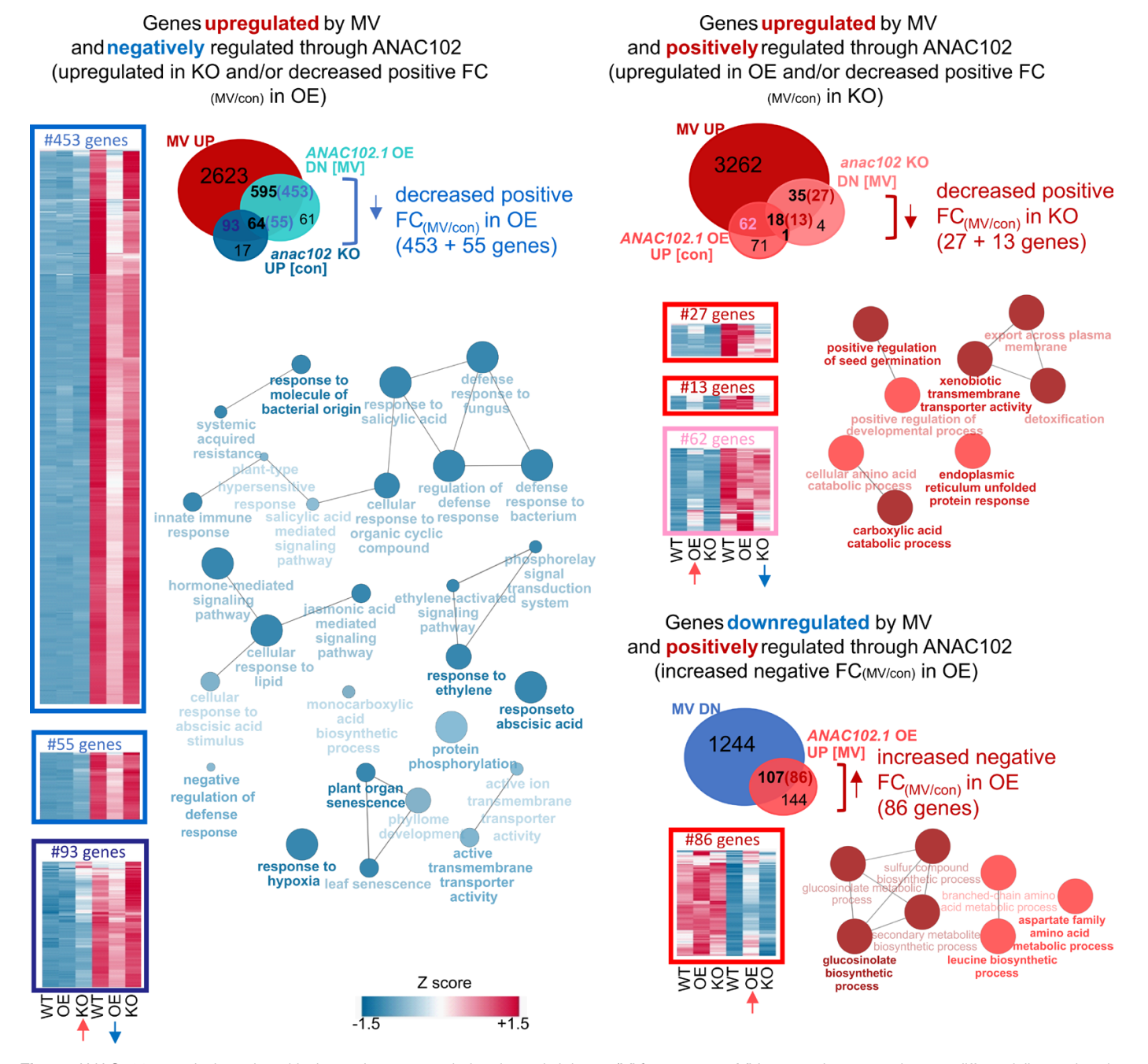


Fig. 4. ANAC102 negatively and positively regulates transcriptional metyl viologen (MV) responses. MV-responsive genes that are differentially regulated through ANAC102 were identified and classified in three clusters based on their up- or downregulation by MV and their positive or negative regulation through ANAC102. Venn diagrams display the number of genes that are regulated by MV in the wild type (WT) (FC >1.5-fold between MV and control in the WT, FDR <0.05) and/or that are differentially regulated by ANAC102 (FC >1.3-fold between ANAC102.1 OE2 or anac102 KO and the WT, FDR <0.05) under control (con) or MV stress conditions. Numbers in parentheses in the Venn diagram intersections indicate genes that in addition have a differential (>1.25) MV-responsive fold change [FC_(MV/con)] between OE2 or KO and WT. Their expression profiles are displayed in heatmaps (Z-score of normalized count data; blue, low expression levels; red, high expression levels) and their functional enrichment [based on biological process Gene Ontology (GO) terms] was analyzed with ClueGO (Bindea et al., 2009). Enrichment significance of the GO term is reflected by the node color (darker color indicating higher significance), and the size of colored nodes indicates the number of genes mapped to each GO term.

to MV (Fig. 3A), we analyzed the genome-wide MV responses 12 h after treatment. The transcript levels of 3375 and 1351 genes were induced and repressed by MV in WT plants, respectively

[fold change (FC) >1.5; false discovery rate (FDR) <0.05]. A significant overlap was observed between MV-induced genes and genes downregulated in ANAC102.1 OE2 versus the

WT under MV stress conditions (659/720 ANAC102.1 OE2 downregulated genes, hypergeometric P-value=0) and/or genes upregulated in anac102 KO lines under control conditions (157/174 anac102 KO upregulated genes, hypergeometric P-value=7.35E-135), indicating that ANAC102 negatively regulates (part of) the MV-induced transcriptome (Fig. 4). Among the 3375 genes induced by MV in the WT, 18% were negatively regulated by ANAC102; that is, having a decreased positive FC_(MV/control) (>1.25-fold difference in FC) and lower MV-induced expression levels in ANAC102.1 OE2 versus the WT (>1.3-fold, FDR <0.05) and/or having higher basal transcript levels in anac102 KO versus the WT (>1.3-fold, FDR <0.05). These MV-induced genes that were negatively regulated through ANAC102 include mitochondrial/chloroplast retrograde target genes, such as AOX1a, SOT12, UGT74E2, UPOX, AT5G43450, AT2G32020, CYP81D8, ABCB4, and AT2G04050, as well as the well-established retrograde regulator ANAC013 (De Clercq et al., 2013). Gene Ontology (GO) enrichment analysis revealed enrichment of various functions, including plant defense response to biotic stress, hormone (salicylic acid, ethylene, jasmonic acid, and abscisic acid) signaling, response to hypoxic stress, and glucosinolate metabolism. Among these differentially expressed genes (DEGs) were 73 TFs, including members of the WRKY and ERF families with functions in biotic stress responses (WRKY48, Xing et al., 2008; and ERF1A, Cheng et al., 2013), as well as TFs involved in abscisic acid signaling (MYB30, Zheng et al., 2012), hypoxia (ERF71, Hess et al., 2011), and glucosinolate catabolism (BGLU28, Zhang et al., 2020).

In addition to MV-induced genes that were negatively regulated by ANAC102, there was a small group of genes (3%) that were upregulated by MV and positively regulated through ANAC102. These genes had elevated basal expression levels in ANAC102.1 OE2 (>1.3 FC, FDR <0.05) and/or showed a reduced MV induction (>1.25-fold difference in FC) and lower MV-induced gene expression levels in anac102 KO versus the WT (>1.3 FC, FDR <0.05). Accordingly, a significant overlap was observed between MV-upregulated genes and genes downregulated in anac102 KO under MV stress (53/58 of the anac102 KO downregulated genes, hypergeometric P-value=8.08E-47) and between MV-upregulated genes and genes that were upregulated in ANAC102.1 OE2 under control conditions (80/152 of the ANAC102.1 OE2 upregulated genes, hypergeometric P-value=6.18E-39) (Fig. 4). These MV-induced genes positively regulated through ANAC102 were enriched for functions in xenobiotic detoxification, transmembrane transport activity, and unfolded protein response (UPR), and included bZIP60 with a well-established function in the regulation of UPR genes, among other TFs (Ye et al., 2011; Moreno et al., 2012).

On the other hand, ANAC102 affected the MV-repressed transcriptome, with 86/1351 (6%) MV-repressed genes being positively regulated by ANAC102; that is, having an increased negative FC_(MV/control) in ANAC102.1 OE2 (>1.25 difference in FC) and increased expression levels in ANAC102.1 OE2 (>1.3 FC, FDR <0.05) versus the WT under MV stress. Accordingly, there was a significant overlap between the MV-downregulated transcriptome and ANAC102.1 OE2 upregulated genes under MV stress (107/251 of ANAC102.1 OE2 upregulated genes, hypergeometric *P*-value=3.75E-80) (Fig. 4). These MV-downregulated genes that were positively regulated through ANAC102 were enriched for functions in glucosinolate biosynthesis and response to insects, and included, among other TFs, MYB29, a regulator of glucosinolate biosynthesis genes that has also been implicated as a negative regulator of retrograde signaling through regulating the complex interplay between hormone and ROS signaling (Gigolashvili et al., 2008; Zhang et al., 2017).

A previous study associated altered Chl content with increased chloroplastic ANAC102 levels in OE lines of the ANAC102.1 CDS fused to a nuclear export sequence (Xin et al., 2021). Since altered Chl content could affect the photosynthesis rate and ROS levels induced by MV, we measured whether our (dual chloroplast-nuclear targeted) ANAC102.1 CDS OE1 and OE2, (nuclear targeted) Met54-gANAC102-GFP OE, and anac102 KO lines also had altered Chl concentrations. Although the Chl content determined after Chl extraction was not significantly altered in any of the ANAC102 mutant lines (Supplementary Fig. S6A), the Chl index estimation (Gitelson et al., 2003) was significantly decreased in ANAC102.1 OE2 and significantly increased in anac102 KO lines relative to the WT (Supplementary Fig. S6B). These results indicate that we cannot exclude that part of the dampened nuclear transcriptional responses to MV is due to the ANAC102.1 OE2 and anac102 KO seedlings being, respectively, more desensitized or sensitized to MV.

In summary, while ANAC102 positively regulates a small subset of the MV-upregulated transcriptome, a substantial portion of the MV-responsive transcriptome was dysregulated in ANAC102.1 OE lines. Specifically, this dysregulation manifests as a diminished induction of MV-upregulated genes and an attenuated repression of MV-downregulated genes.

ANAC102 regulates transcriptional methyl viologen responses directly and indirectly through downstream transcription factor networks

To investigate the underlying mechanisms governing the differential regulation of MV responses in ANAC102 gainand loss-of-function lines, we sought to determine whether ANAC102 exerts direct transcriptional control or if its influence is mediated indirectly through downstream TF networks. We conducted an analysis by intersecting DEGs with the direct target genes identified through ANAC102 ChIP-seq analysis (Song et al., 2016) (peak annotation procedure detailed in the Materials and methods). Among the MV-induced genes that were negatively regulated by ANAC102, 50% were also identified as direct target genes in the ChIP-seq dataset. Similarly,

52% of the genes that were positively regulated by ANAC102 during MV induction and 24% of the genes that were positively regulated by ANAC102 during MV repression overlapped with ANAC102 ChIP-seq target genes. These observations suggest that a substantial portion of the MV-responsive transcriptome under ANAC102 regulation may be directly modulated through ANAC102's binding to the promoters. Since the overlap between ANAC102-regulated DEGs and ChIP-seq data revealed 39 TFs, we explored whether these TFs could act as intermediates in regulating the ANAC102-regulated transcriptome under MV stress. Using TF2Network, which predicts TFs for a set of target genes based on motif enrichment. TF-target gene co-expression, and experimental protein-DNA binding data (Kulkarni et al., 2018), we predicted 24 of these TFs to regulate a subset of the ANAC102-regulated transcriptome during MV stress (Supplementary Fig. S7). Similarly,

employing a more advanced gene regulatory network approach that integrates DNA motif, open chromatin, TF binding, and co-expression information using machine learning [referred to as integrated gene regulatory network (iGRN), De Clercq et al. (2021)], we predicted 34 of these 39 ANAC102-regulated TFs as regulators of ANAC102 DEGs, with 10 TFs (CZF1, WRKY75, WRKY48, ERF-1, SCL13, WRKY40, ZAT6, RHL41, WRKY6, and STZ) among the 20 most enriched TFs, and CZF1, WRKY75, and WRKY48 ranked first, third, and fourth, respectively (Fig. 5). Interestingly, 17 TFs were predicted by both TF2Network and iGRN (WRKY75, WRKY48, ERF-1, WRKY40, WRKY6, WRKY11, ERF5, WRKY45, WRKY28, ERF4, ANAC062, WRKY22, ORA47, DOF1, CBF2, ABR1, and MYB30), indicating, that in addition to direct transcriptional regulation of target genes, ANAC102 also plays a role in orchestrating downstream TF regulatory

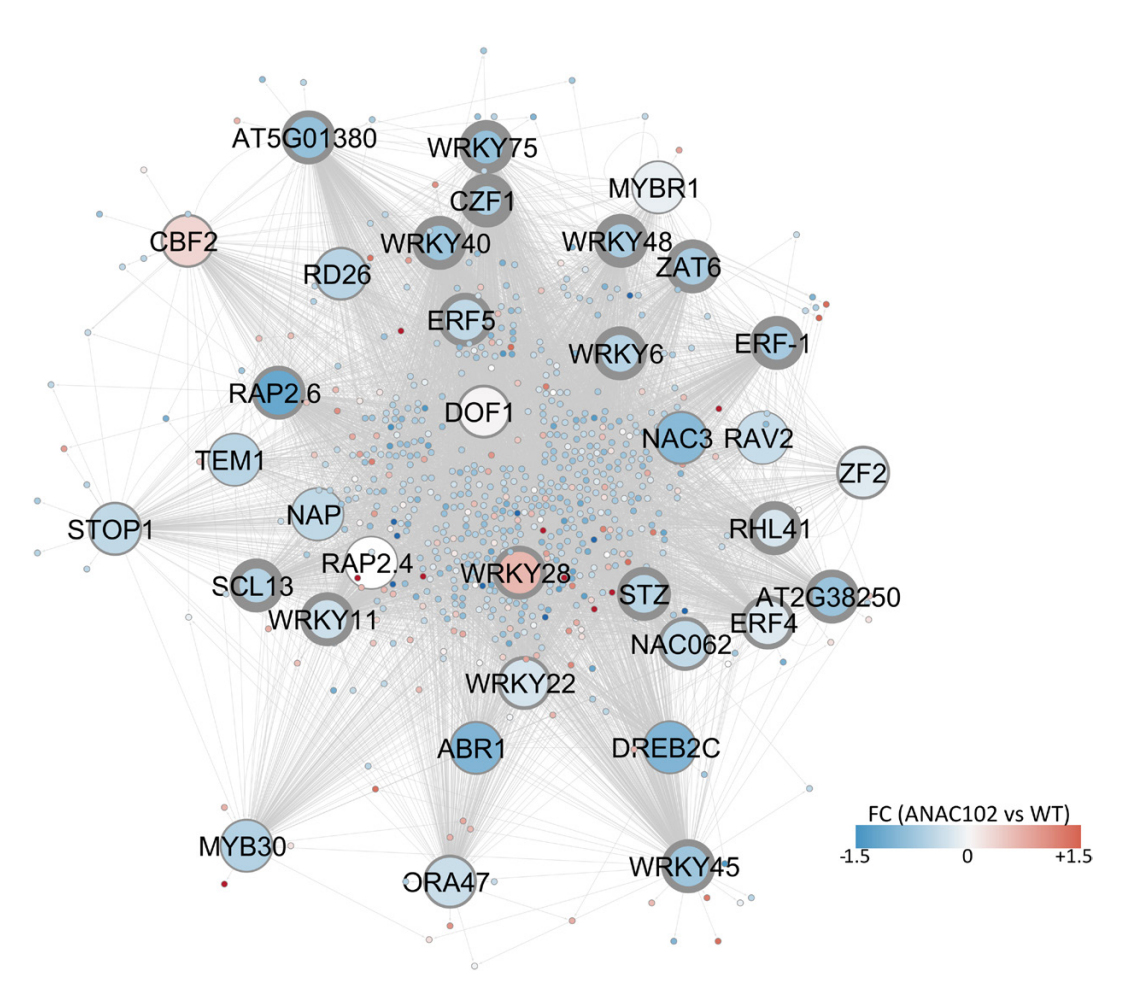


Fig. 5. Transcriptional regulatory networks mediating metyl viologen (MV) responses downstream of ANAC102. To construct transcriptional regulatory networks modulated by ANAC102 in response to MV stress, we identified MV-responsive TFs exhibiting differential expression in ANAC102.1 OE2 and/ or anac102 KO (RNA-seq) that were also classified as direct ANAC102 targets based on ChIP-seq analysis (Song et al., 2016) and that were additionally predicted by iGRN (De Clercg et al., 2021) as regulators of ANAC102 DEGs. The TF (large nodes)-target gene (small nodes) interactions were displayed with Cytoscape 3.8.2 (Shannon et al., 2003). The thickness of the TF node border lines indicates enrichment statistics [q-value based on hypergeometric distribution combined with Benjamini-Hochberg correction (De Clercq et al., 2021)] of TF association with the target genes. Node color indicates the fold change in ANAC102.1 OE2 compared to the WT under MV stress or the negative FC of anac102 KO compared to the WT under MV stress, with blue indicating negative and red indicating positive regulation by ANAC102.

networks, by primarily exerting negative regulation of these networks (Fig. 5).

Among the putative intermediate TFs were several TFs with functions in plant abiotic and biotic stress responses and, more specifically, with functions related to ANAC102. For example, SALT TOLERANCE ZINC FINGER (STZ), analogous to ANAC102, has a positive regulatory role in photooxidative stress responses (Rossel et al., 2007). In addition, WRKY40 and WRKY45 confer tolerance to hypoxia through retrograde signaling and are involved in age-triggered leaf senescence, and both these functions were enriched among the MV-upregulated genes that were negatively regulated by ANAC102 (Fig. 5) (Chen et al., 2017; Meng et al., 2020). SCARECROW-LIKE 13 (SCL13) is a positive regulator of phytochrome-dependent red light signaling (Torres-Galea et al., 2006). Interestingly, ANAC102 transcription initiation is differentially regulated by phytochrome-mediated alternative promoter selection in response to red light, and its closest homolog, ATAF2, has been implicated in photomorphogenesis (Ushijima et al., 2017). Moreover, several of the identified TFs have functions in response to microbial pathogens [for example, WRKY11, Jiang et al. (2016) and WRKY48, Xing et al. (2008)]. Although the role of ANAC102 in response to biotic stress factors has to our knowledge not been studied, many of its DEGs are involved in biotic stress responses and glucosinolate biosynthesis (Fig. 4). However, its close relatives, ATAF1 and ATAF2, have wellestablished functions in defense responses, and ATAF2 has also been implicated in the response to wounding (Delessert et al., 2005; Wang et al., 2009).

Discussion

ANAC102 mainly expresses a nuclear proteoform without the complete N-terminal chloroplast-targeting peptide

In this study, our primary objective was to clarify the subcellular localization of ANAC102, which has previously been implicated in orchestrating plant responses to various stresses (Christianson et al., 2009; D'Alessandro et al., 2018; Han et al., 2023). Previous studies investigating the annotated ANAC102 coding sequences (ANAC102.1 and ANAC102.2) driven by a constitutive promoter underlined its localization and function in chloroplasts (Inzé et al., 2012; Xin et al., 2021). Our study, however, used the full genomic ANAC102 sequence including its 5' regulatory region and 5'UTR, and revealed under both control and stress conditions only a single protein isoform that lacked a complete N-terminal cTP and was exclusively localized to the nucleus (Fig. 1; Supplementary Fig. S2). This proteoform probably originated from the first TIS (Met54) downstream of a TSS identified by TSS-Seq (Ushijima et al., 2017; Nielsen et al., 2019) and previously identified by RiboSeq profiling (Willems et al., 2022). However, since our and other recent studies (Cresta and D'Alessandro, 2023; Han et al., 2023) additionally detected a larger, 5'-extended mRNA isoform, albeit at very low concentrations, we cannot exclude the possibility that a proteoform with a complete, functional cTP also exists. When we enforced transcription of ANAC102 from a more upstream start codon through a constitutive promoter (p35S::Met11-gANAC102-GFP), we observed both a nuclear and chloroplast localization, as Xin et al. (2021) did. However, it remains unclear how the dual localization is achieved and whether the nuclear isoform is obtained after relocalization of the chloroplast-imported protein or is the result of dual targeting of the full-length protein from the cytosol, as was observed for SWIB-4 (Melonek et al., 2012). Although the two inframe, downstream AUGs (Met54 and Met108) in the Met11gANAC102-GFP construct were mutated, we cannot exclude that a cTP-depleted, nuclear isoform is generated directly as a result of alternative (non-AUG) translation initiation downstream of Met11. Nevertheless, a constitutive promoter driving the expression of a particular transcript model might not be representative of the actual physiological situation. To conclude, our study supports that ANAC102 primarily expresses a nuclear isoform and therefore mainly exerts a function in the nucleus. This is in agreement with a recent study showing a function of ANAC102 as a direct transcriptional activator of a nuclear Cd-responsive gene (Han et al., 2023).

ANAC102 overexpression increases sensitivity to methyl viologen-induced chloroplast oxidative stress

ANAC102 was previously identified as a regulator of lowoxygen-, Cd-, and β-cc-mediated photooxidative stress responses, exerting a positive effect on tolerance to these stresses (Christianson et al., 2009; D'Alessandro et al., 2018; Han et al., 2023). Accordingly, ANAC102 transcript levels were induced under these stress conditions. However, the induction by Cd and β -cc was not uniform throughout the plant, but was restricted to the root and young leaves, respectively. In our previous study, we reported an altered growth phenotype by ANAC102 overexpression after germination and growth under mild (nanomolar range) MV stress, with contradictory phenotypes depending on the overexpression levels (De Clercq et al., 2021). Here, we show that both weak and strong ANAC102 OE lines are more sensitive to long-term, more severe (micromolar range) MV stress, resulting in an accelerated cell death phenotype (Fig. 2). Moreover, our findings reveal that ANAC102 overexpression partially suppresses the upregulation of MV-induced genes, including a set of well-established retrograde target genes, potentially through direct binding to their promoters (Fig. 3). These retrograde target genes, previously referred to as MDS genes, include members of the cytochrome P450 monooxygenases, glutathione S-transferases, UDP-glucosyl transferases, and transmembrane transporters, which have putative functions in detoxification and transport of toxic and/or reactive molecules. Moreover, the MDS genes are direct targets of ANAC013 and ANAC017, which are known

to positively affect plant MV tolerance (De Clercq et al., 2013; Van Aken et al., 2016). In contrast, our transcriptome analysis as well as the study by D'Alessandro et al. (2018) show that ANAC102 also positively regulates a subset of genes involved in detoxification responses. Taken together, our and previous studies highlight the complex role of ANAC102 in finetuning plant responses to environmental challenges, especially to stresses that generate reactive molecules, such as hypoxia, heavy metals, excess light, and chemicals that induce the generation of ROS in chloroplasts. However, our study opens a new perspective for the understanding of ANAC102's function, which might act not only as an activator of stress responses, but also as a repressor, depending on the promoter context or the severity and/or nature of the stress conditions. A previous study indicated that ANAC102 is mainly induced in young leaves, and that the β-cc-mediated detoxification responses regulated through SCL14, and potentially ANAC102, contribute to the protection and higher resistance of young leaves to high-light stress (D'Alessandro et al., 2018). In contrast, in our MV stress assays, we observed an increased sensitivity of young leaves compared to older leaves, leading to a faster decline in photosynthetic activity and accelerated cell death (Fig. 2). Moreover, the MV sensitivity of young leaves is more pronounced in ANAC102 OE lines compared to the WT, suggesting that under severe MV stress, ANAC102 might negatively modulate detoxification responses in young tissues. Altogether, our study highlights the complex role of ANAC102 in the positive and negative regulating detoxification responses depending on the type and severity of stress and the specific tissue and/or developmental stage of the plant.

ANAC102 regulates metyl viologen-induced chloroplast retrograde responses in the nucleus

Previous studies have demonstrated that changes in ANAC102 levels impact nuclear expression, particularly of those genes involved in the response to low oxygen and metal stress, detoxification during photooxidative stress, and brassinosteroid metabolism during seedling photomorphogenesis (Christianson et al., 2009; D'Alessandro et al., 2018; Peng and Neff, 2020; Han et al., 2023). Moreover, the promoters of genes differentially expressed by ANAC102 overexpression have been found to over-represent a NAC consensus binding site, suggesting that ANAC102 directly regulates gene expression in the nucleus (Christianson et al., 2009). Furthermore, ANAC102 has been shown to activate a nuclear gene involved in Cd stress tolerance by binding directly to its promoter (Han et al., 2023). In this study, we further confirmed the nuclear function of ANAC102 by demonstrating that ANAC102 binds to the promoters of the MDS retrograde target genes in the Y1H system, we well as by comparative analysis of the ANAC102-regulated MV-responsive transcriptome and the nuclear ANAC102 target genes identified by ChIP-seq analysis. However, we cannot exclude that part of the altered MV-responsive transcriptome by

ANAC102 overexpression or knockout is indirect and a result of physiological changes from altered ANAC102 expression; for example, altered Chl levels in ANAC102 OE and KO lines (Xin et al., 2021) (Supplementary Fig. S6) could affect light absorption, and thereby (de)sensitize plants to MV.

Our transcriptome analysis further unraveled a dual role of ANAC102 in modulating genome-wide transcriptional responses to MV stress by mediating both negative and positive regulation, thereby influencing the MV-driven up- and downregulation of a diverse set of genes (Fig. 4). This dual regulatory function suggests a sophisticated mechanism by which ANAC102 acts as both a transcriptional activator and a repressor, and this might depend on the promoter context, growth/stress conditions, and/or the specific tissue and developmental stage of the plants. Similarly, its close relative, ATAF2, has been shown to act as an activator or repressor, activating or repressing PATHOGENESIS-RELATED GENE expression, depending on the specific growth conditions and developmental stage of the plants (Delessert et al., 2005; Wang et al., 2009). Although we observed a substantial overlap between the ANAC102 negatively regulated genes and the ANAC102 target genes identified by ChIP-seq, a transcriptional repressor function remains to be demonstrated. ANAC102 has previously been shown to suppress the expression of two brassinosteroid catabolic genes, but this was not through direct promoter binding, but probably through protein-protein interactions with ATAF2 and CCA1, which act as direct repressors of these genes (Peng et al., 2015; Peng and Neff, 2020). Thus, part of the complex regulatory mechanisms of ANAC102 may occur through the formation of homo- and heterodimers among the ATAFs and with other TFs such as CCA1. Interestingly, several of the ANAC102-regulated DEGs identified during MV responses overlapped with ATAF2 target genes identified under control and wounding stress conditions (Delessert et al., 2005). As we have previously observed contradictory phenotypes between weak and strong ANAC102 OE lines during mild MV stress (De Clercq et al., 2021), ANAC102 might act as an activator or repressor in a dose-dependent manner. Similarly, the *Drosophila* zinc finger TF KRUPPEL can have opposite regulatory effects on the expression of a single gene in a concentration-dependent manner, converting from an activator to a repressor at higher concentrations through homodimer formation (Sauer and Jäckle, 1993).

Together, our ChIP-seq analysis and reverse engineering of TF networks indicate that ANAC102 influences the MV responses via both direct regulatory interactions and indirectly through downstream TFs, most of which (Fig. 5) are negatively regulated by ANAC102. Several of these TFs could contribute to reported ANAC102 functions, including photooxidative and hypoxia stress responses (Rossel et al., 2007; Meng et al., 2020). This complex regulatory network provides insights into the putative role of ANAC102 as a master regulator in modulating plant responses to various environmental challenges. To summarize, our study suggests a sophisticated mechanism by

4668 | Luo et al.

which ANAC102 fine-tunes the plant's transcriptional landscape during various stresses through a dual activator and repressor function and by regulating downstream TF regulatory networks.

Supplementary data

The following supplementary data are available at *JXB* online. Fig. S1. Quantification cycle (Cq) values of the reference genes in the RT-qPCR samples.

Fig. S2. Subcellular localization of gANAC102–GFP and comparison with N-terminal truncated gANAC102 proteoforms.

Fig. S3. Ribosome profiling results of ANAC102 translation initiation sites according to Willems *et al.* (2022).

Fig. S4. Phenotype of *Met54-gANAC102-GFP* OE plants under MV-induced oxidative stress.

Fig. S5. MDS gene expression in the Met54-ANAC102-GFP OE line.

Fig. S6. Total chlorophyll content and chlorophyll index of WT and *ANAC102* OE and KO lines.

Fig. S7. Construction of the transcriptional regulatory network mediating MV responses downstream of ANAC102 using TF2Network.

Table S1. List of primers used in this study.

Acknowledgements

The authors thank Karin Krupinska and Rena Isemer (Kiel University) and Alain Goossens and Issl Kimpe (Ghent University) for the help with experimental assays and scientific discussions related to this research; Franziska Turck (Max Planck Institute, Cologne) for providing the REGIA TF library; Annelies Inzé and Sandy Vanderauwera for sharing *ANAC102.1* OE1 and OE2 lines; Patrick Willems for help with the Ribo-seq data analysis; Kris Audenaert, Noémie De Zutter, and Siel Goethals (Ghent University) for help with chlorophyll index measurements; and Annick Bleys for help with the manuscript.

Author contributions

IDC, FVB, and XL: designing the research; IDC and XL: designing the experiments and data analysis; XL, IDC, XJ, VS, HCT, and SMK: performing the experiments; HCT and OVA: RNA-seq raw data analysis; SRK and KV: ChIP-seq data analysis; IDC: downstream bio-informatic analyses; IDC and XL: writing with input of all co-authors.

Conflict of interest

The authors declare no conflict of interest.

Funding

This work was funded by the European Research Council under the Horizon 2020 research and Innovation Program (grant agreement

no. 949808) to IDC, the China Scholarship Council (PhD fellowship 201706910099) and the Special Research Fund (BOF; Ghent University, grant no. 01CD1323) to XL, the Research Foundation-Flanders (grant no. G007723N to FVB and grant no. G001015N to KV).

Data availability

The data supporting the findings of this study are available from the corresponding author upon request.

References

Arnon DI. 1949. Copper enzymes in isolated chloroplasts. Polyphenoloxidase in *Beta vulgaris*. Plant Physiology **24**, 1–15.

Baxter A, Mittler R, Suzuki N. 2014. ROS as key players in plant stress signalling. Journal of Experimental Botany **65**, 1229–1240.

Bindea G, Mlecnik B, Hackl H, Charoentong P, Tosolini M, Kirilovsky A, Fridman W-H, Pagès F, Trajanoski Z, Galon J. 2009. ClueGO: a Cytoscape plug-in to decipher functionally grouped gene ontology and pathway annotation networks. Bioinformatics 25, 1091–1093.

Chen L, Xiang S, Chen Y, Li D, Yu D. 2017. *Arabidopsis* WRKY45 interacts with the DELLA protein RGL1 to positively regulate age-triggered leaf senescence. Molecular Plant 10, 1174–1189.

Cheng M-C, Liao P-M, Kuo W-W, Lin T-P. 2013. The *Arabidopsis* ETHYLENE RESPONSE FACTOR1 regulates abiotic stress-responsive gene expression by binding to different cis-acting elements in response to different stress signals. Plant Physiology **162**, 1566–1582.

Christianson JA, Wilson IW, Llewellyn DJ, Dennis ES. 2009. The low-oxygen-induced NAC domain transcription factor *ANAC102* affects viability of *Arabidopsis* seeds following low-oxygen treatment. Plant Physiology **149**, 1724–1738.

Clough SJ, Bent AF. 1998. Floral dip: a simplified method for *Agrobacterium*-mediated transformation of *Arabidopsis thaliana*. The Plant Journal **16**, 735–743.

Considine MJ, Foyer CH. 2021. Oxygen and reactive oxygen species-dependent regulation of plant growth and development. Plant Physiology **186**, 79–92.

Crawford T, Lehotai N, Strand A. 2018. The role of retrograde signals during plant stress responses. Journal of Experimental Botany **69**, 2783–2795.

Cresta A, D'Alessandro S. 2023. Arabidopsis *ANAC102*, chloroplastic or nucleocytosolic localization? Genes **14**, 438.

D'Alessandro S, Ksas B, Havaux M. 2018. Decoding β -cyclocitral-mediated retrograde signaling reveals the role of a detoxification response in plant tolerance to photooxidative stress. The Plant Cell **30**, 2495–2511.

De Clercq I, Van de Velde J, Luo X, Liu L, Storme V, Van Bel M, Pottie R, Vaneechoutte D, Van Breusegem F, Vandepoele K. 2021. Integrative inference of transcriptional networks in *Arabidopsis* yields novel ROS signalling regulators. Nature Plants 7, 500–513.

De Clercq I, Vermeirssen V, Van Aken O, et al. 2013. The membrane-bound NAC transcription factor ANAC013 functions in mitochondrial retrograde regulation of the oxidative stress response in *Arabidopsis*. The Plant Cell **25**, 3472–3490.

Delessert C, Kazan K, Wilson IW, Van Der Straeten D, Manners J, Dennis ES, Dolferus R. 2005. The transcription factor ATAF2 represses the expression of pathogenesis-related genes in Arabidopsis. The Plant Journal **43**, 745–757.

Deplancke B, Vermeirssen V, Arda HE, Martinez NJ, Walhout AJM. 2006. Gateway-compatible yeast one-hybrid screens. Cold Spring Harbor Protocols **2006**, pdb.prot4590.

Dietz K-J, Turkan I, Krieger-Liszkay A. 2016. Redox- and reactive oxygen species-dependent signaling into and out of the photosynthesizing chloroplast. Plant Physiology **171**, 1541–1550.

- Dobin A, Davis CA, Schlesinger F, Drenkow J, Zaleski C, Jha S, Batut P. Chaisson M. Gingeras TR. 2013. STAR: ultrafast universal RNA-seq aligner. Bioinformatics 29, 15-21.
- Estavillo GM. Crisp PA. Pornsiriwong W. et al. 2011. Evidence for a SAL1-PAP chloroplast retrograde pathway that functions in drought and high light signaling in Arabidopsis. The Plant Cell 23, 3992-4012.
- Exposito-Rodriguez M, Laissue PP, Yvon-Durocher G, Smirnoff N, Mullineaux PM. 2017. Photosynthesis-dependent H₂O₂ transfer from chloroplasts to nuclei provides a high-light signalling mechanism. Nature Communications 8, 49.
- Gechev TS, Van Breusegem F, Stone JM, Denev I, Laloi C. 2006. Reactive oxygen species as signals that modulate plant stress responses and programmed cell death. Bioessays 28, 1091-1101.
- Gigolashvili T, Engqvist M, Yatusevich R, Müller C, Flügge U-I. 2008. HAG2/MYB76 and HAG3/MYB29 exert a specific and coordinated control on the regulation of aliphatic glucosinolate biosynthesis in Arabidopsis thaliana. New Phytologist 177, 627-642.
- Gitelson AA, Gritz Y, Merzlyak MN. 2003. Relationships between leaf chlorophyll content and spectral reflectance and algorithms for nondestructive chlorophyll assessment in higher plant leaves. Journal of Plant Physiology 160, 271-282.
- Han GH, Huang RN, Hong LH, Xu JX, Hong YG, Wu YH, Chen WW. 2023. The transcription factor NAC102 confers cadmium tolerance by regulating WAKL11 expression and cell wall pectin metabolism in Arabidopsis. Journal of Integrative Plant Biology 65, 2262-2278.
- Hess N, Klode M, Anders M, Sauter M. 2011. The hypoxia responsive transcription factor genes ERF71/HRE2 and ERF73/HRE1 of Arabidopsis are differentially regulated by ethylene. Physiologia Plantarum 143, 41-49.
- Inzé A. 2012. Protein subcellular trafficking during the oxidative stress response in plants. PhD thesis, Ghent University.
- Inzé A, Vanderauwera S, Hoeberichts FA, Vandorpe M, Van Gaever T, Van Breusegem F. 2012. A subcellular localization compendium of hydrogen peroxide-induced proteins. Plant, Cell & Environment 35, 308-320.
- Jiang C-H, Huang Z-Y, Xie P, et al. 2016. Transcription factors WRKY70 and WRKY11 served as regulators in rhizobacterium Bacillus cereus AR156induced systemic resistance to Pseudomonas syringae pv. tomato DC3000 in Arabidopsis. Journal of Experimental Botany 67, 157-174.
- Karimi M, Inzé D, Depicker A. 2002. GATEWAY™ vectors for Agrobacterium-mediated plant transformation. Trends in Plant Science 7, 193-195.
- Kulkarni SR, Vaneechoutte D, Van de Velde J, Vandepoele K. 2018. TF2Network: predicting transcription factor regulators and gene regulatory networks in Arabidopsis using publicly available binding site information. Nucleic Acids Research 46, e31.
- Li X. 2011. Infiltration of Nicotiana benthamiana protocol for transient expression via Agrobacterium. Bio-protocol 1, e95.
- Liao Y, Smyth GK, Shi W. 2014. featureCounts: an efficient general purpose program for assigning sequence reads to genomic features. Bioinformatics 30, 923-930.
- Livak KJ, Schmittgen TD. 2001. Analysis of relative gene expression data using real-time quantitative PCR and the $2^{-\Delta\Delta CT}$ method. Methods 25,
- Love MI. Huber W. Anders S. 2014. Moderated estimation of fold change and dispersion for RNA-seq data with DESeq2. Genome Biology 15, 550.
- Melonek J, Matros A, Trösch M, Mock H-P, Krupinska K. 2012. The core of chloroplast nucleoids contains architectural SWIB domain proteins. The Plant Cell 24, 3060-3073.
- Meng X, Li L, Narsai R, De Clercq I, Whelan J, Berkowitz O. 2020. Mitochondrial signalling is critical for acclimation and adaptation to flooding in Arabidopsis thaliana. The Plant Journal 103, 227-247.
- Mittler R, Zandalinas SI, Fichman Y, Van Breusegem F. 2022. Reactive oxygen species signalling in plant stress responses. Nature Reviews. Molecular Cell Biology 23, 663-679.
- Moreno AA, Mukhtar MS, Blanco F, et al. 2012. IRE1/bZIP60-mediated unfolded protein response plays distinct roles in plant immunity and abiotic stress responses. PLoS One 7, e31944.

- Moulin M, McCormac AC, Terry MJ, Smith AG. 2008. Tetrapyrrole profiling in Arabidopsis seedlings reveals that retrograde plastid nuclear signaling is not due to Mg-protoporphyrin IX accumulation. Proceedings of the National Academy of Sciences, USA 105, 15178-15183.
- Nielsen M, Ard R, Leng X, Ivanov M, Kindgren P, Pelechano V, Marquardt S. 2019. Transcription-driven chromatin repression of intragenic transcription start sites. PLoS Genetics 15, e1007969.
- Paz-Ares J; Regia Consortium. 2002. REGIA, an EU project on functional genomics of transcription factors from Arabidopsis thaliana. Comparative and Functional Genomics 3, 102-108.
- Peng H. Neff MM. 2020. CIRCADIAN CLOCK ASSOCIATED 1 and ATAF2 differentially suppress cytochrome P450-mediated brassinosteroid inactivation. Journal of Experimental Botany 71, 970-985.
- Peng H, Zhao J, Neff MM. 2015. ATAF2 integrates Arabidopsis brassinosteroid inactivation and seedling photomorphogenesis. Development 142, 4129-4138
- Ramel F, Birtic S, Ginies C, Soubigou-Taconnat L, Triantaphylidès C, Havaux M. 2012. Carotenoid oxidation products are stress signals that mediate gene responses to singlet oxygen in plants. Proceedings of the National Academy of Sciences, USA 109, 5535-5540.
- Rossel JB, Wilson PB, Hussain D, Woo NS, Gordon MJ, Mewett OP, Howell KA, Whelan J, Kazan K, Pogson BJ. 2007. Systemic and intracellular responses to photooxidative stress in Arabidopsis. The Plant Cell **19**, 4091–4110.
- Sauer F, Jäckle H. 1993. Dimerization and the control of transcription by Kruppel. Nature 364, 454-457.
- Schwenkert S, Fernie AR, Geigenberger P, Leister D, Möhlmann T, Naranjo B, Neuhaus HE. 2022. Chloroplasts are key players to cope with light and temperature stress. Trends in Plant Science 27, 577-587.
- Shannon P, Markiel A, Ozier O, Baliga NS, Wang JT, Ramage D, Amin N, Schwikowski B, Ideker T. 2003. Cytoscape: a software environment for integrated models of biomolecular interaction networks. Genome Research 13, 2498-2504.
- Song L, Huang SC, Wise A, Castanon R, Nery JR, Chen H, Watanabe M, Thomas J, Bar-Joseph Z, Ecker JR. 2016. A transcription factor hierarchy defines an environmental stress response network. Science 354. aaq1550.
- Terry MJ, Smith AG. 2013. A model for tetrapyrrole synthesis as the primary mechanism for plastid-to-nucleus signaling during chloroplast biogenesis. Frontiers in Plant Science 4, 14.
- Torres-Galea P, Huang L-F, Chua N-H, Bolle C. 2006. The GRAS protein SCL13 is a positive regulator of phytochrome-dependent red light signaling. but can also modulate phytochrome A responses. Molecular Genetics and Genomics 276, 13-30.
- Ugalde JM, Fuchs P, Nietzel T, Cutolo EA, Homagk M, Vothknecht UC, Holuique L, Schwarzländer M, Müller-Schüssele SJ, Meyer AJ. 2021. Chloroplast-derived photo-oxidative stress causes changes in H₂O₂ and E_{GSH} in other subcellular compartments. Plant Physiology 186, 125-141.
- Ushijima T, Hanada K, Gotoh E, et al. 2017. Light controls protein localization through phytochrome-mediated alternative promoter selection. Cell 171, 1316-1325.e12.
- Van Aken O, De Clercq I, Law SR, Van Breusegem F, Millar AH, Whelan J. 2016. Mitochondrial and chloroplast stress responses are modulated in distinct touch and chemical inhibition phases. Plant Physiology **171**, 2150–2165.
- Vermeirssen V, Deplancke B, Barrasa MI, et al. 2007. Matrix and Steiner-triple-system smart pooling assays for high-performance transcription regulatory network mapping. Nature Methods 4, 659-664.
- Wang X, Goregaoker SP, Culver JN. 2009. Interaction of the Tobacco mosaic virus replicase protein with a NAC domain transcription factor is associated with the suppression of systemic host defenses. Journal of Virology 83, 9720-9730.
- Willems P, Ndah E, Jonckheere V, Van Breusegem F, Van Damme P. 2022. To new beginnings: riboproteogenomics discovery of N-terminal proteoforms in Arabidopsis thaliana. Frontiers in Plant Science 12, 778804.

4670 | Luo et al.

Woodson JD, Chory J. 2008. Coordination of gene expression between organellar and nuclear genomes. Nature Reviews. Genetics **9**, 383–395.

Xiao Y, Savchenko T, Baidoo EEK, Chehab WE, Hayden DM, Tolstikov V, Corwin JA, Kliebenstein DJ, Keasling JD, Dehesh K. 2012. Retrograde signaling by the plastidial metabolite MEcPP regulates expression of nuclear stress-response genes. Cell 149, 1525–1535.

Xin K, Pan T, Gao S, Yan S. 2021. A transcription factor regulates gene expression in chloroplasts. International Journal of Molecular Sciences 22, 6769.

Xing D-H, Lai Z-B, Zheng Z-Y, Vinod KM, Fan B-F, Chen Z-X. 2008. Stress- and pathogen-induced *Arabidopsis* WRKY48 is a transcriptional activator that represses plant basal defense. Molecular Plant 1, 459–470.

Ye C, Dickman MB, Whitham SA, Payton M, Verchot J. 2011. The unfolded protein response is triggered by a plant viral movement protein. Plant Physiology **156**, 741–755.

Zhang X, Ivanova A, Vandepoele K, et al. 2017. The transcription factor MYB29 is a regulator of *ALTERNATIVE OXIDASE1a*. Plant Physiology **173**, 1824–1843.

Zhang L, Kawaguchi R, Morikawa-Ichinose T, Allahham A, Kim S-J, Maruyama-Nakashita A. 2020. Sulfur deficiency-induced glucosinolate catabolism attributed to two β -glucosidases, BGLU28 and BGLU30, is required for plant growth maintenance under sulfur deficiency. Plant and Cell Physiology **61**, 803–813.

Zheng Y, Schumaker KS, Guo Y. 2012. Sumoylation of transcription factor MYB30 by the small ubiquitin-like modifier E3 ligase SIZ1 mediates abscisic acid response in *Arabidopsis thaliana*. Proceedings of the National Academy of Sciences, USA **109**, 12822–12827.

Zimmermann P, Hirsch-Hoffmann M, Hennig L, Gruissem W. 2004. GENEVESTIGATOR. Arabidopsis microarray database and analysis toolbox. Plant Physiology **136**, 2621–2632.